Effect of impellers configuration on the gas dispersion in high-viscosity fluid using narrow annular gap unit. Part 1: Experimental approach

Kaies Souidi, Anamaria Mardaru, Matthieu Roudet, Alain Marcati, Dominique Della Valle, Gholamreza Djelveh

XML-IS

Our reference: CES 10322 P-authorquery-vx

AUTHOR QUERY FORM

ELSEVIER	**Journal: CES** **Article Number: 10322**	**Please e-mail or fax your responses and any corrections to:** **E-mail: corrections.essd@elsevier.macipd.com** **Fax: +44 1392 285878**

Dear Author,

Please check your proof carefully and mark all corrections at the appropriate place in the proof (e.g., by using on-screen annotation in the PDF file) or compile them in a separate list. Note: if you opt to annotate the file with software other than Adobe Reader then please also highlight the appropriate place in the PDF file. To ensure fast publication of your paper please return your corrections within 48 hours.

For correction or revision of any artwork, please consult http://www.elsevier.com/artworkinstructions.

Any queries or remarks that have arisen during the processing of your manuscript are listed below and highlighted by flags in the proof. Click on the Q link to go to the location in the proof.

Location in article	Query / Remark: click on the Q link to go Please insert your reply or correction at the corresponding line in the proof
Q1	Please confirm that given names and surnames have been identified correctly.

Thank you for your assistance.

Chemical Engineering Science ▮ (▮▮▮▮) ▮▮▮–▮▮▮

Contents lists available at SciVerse ScienceDirect

Chemical Engineering Science

journal homepage: www.elsevier.com/locate/ces

Highlights

Effect of impellers configuration on the gas dispersion in high-viscosity fluid using narrow annular gap unit. Part 1: Experimental approach

Q1 K. Souidi [a], A. Mardaru [a,c], M. Roudet [a,b], A. Marcati [a,b], D. Della Valle [d,e], G. Djelveh [a,b]

[a] CNRS, UMR 6602, Institut Pascal, F-63177 Aubière, Puy de dome, France
[b] Clermont Université, ENSCCF, Institut Pascal, BP 10448, F-63000, Clermont-Ferrand, France
[c] University POLITEHNICA of Bucharest, Chemical Engineering Department, Polizu St., No.1-6, Bucharest, Romania
[d] LTN-UMR-CNRS 6602, École Polytechnique de l'Université de Nantes, rue Christian Pauc, 44306 Nantes, France
[e] ONIRIS, rue de la Géraudière, BP82225, 44322 cedex 3, Nantes, France

► Impact of impeller configuration on gas dispersion efficiency in food raw material. ► Power consumption is not correlated to the gas dispersion efficiency. ► Shifted paddles enhance dispersion efficiency. ► Bubble size distribution is independent of the impeller configuration. ► Tip streaming is the dominant mechanism of bubble breakup in such raw material.

0009-2509/$ - see front matter © 2012 Published by Elsevier Ltd.
doi:10.1016/j.ces.2012.02.055

Please cite this article as: Souidi, K., et al., Effect of impellers configuration on the gas dispersion in high-viscosity fluid using narrow annular gap unit. Part 1: Experimental approach. Chem. Eng. Sci. (2012), doi:10.1016/j.ces.2012.02.055

Chemical Engineering Science ▮ (▮▮▮▮) ▮▮▮–▮▮▮

Contents lists available at SciVerse ScienceDirect

Chemical Engineering Science

journal homepage: www.elsevier.com/locate/ces

Effect of impellers configuration on the gas dispersion in high-viscosity fluid using narrow annular gap unit. Part 1: Experimental approach

Q1 K. Souidi[a], A. Mardaru[a,c], M. Roudet[a,b], A. Marcati[a,b], D. Della Valle[d,e], G. Djelveh[a,b,*]

[a] CNRS, UMR 6602, Institut Pascal, F-63177 Aubière, Puy de dome, France
[b] Clermont Université, ENSCCF, Institut Pascal, BP 10448, F-63000, Clermont-Ferrand, France
[c] University POLITEHNICA of Bucharest, Chemical Engineering Department, Polizu St., No.1-6, Bucharest, Romania
[d] LTN-UMR-CNRS 6602, École Polytechnique de l'Université de Nantes, rue Christian Pauc, 44306 Nantes, France
[e] ONIRIS, rue de la Géraudière, BP82225, 44322 cedex 3, Nantes, France

ARTICLE INFO

Article history:
Received 25 November 2011
Received in revised form
15 February 2012
Accepted 29 February 2012

Keywords:
Food processing
Foam
Imaging
Laminar flow
Bubble
Hydrodynamics

ABSTRACT

The effect of impellers configuration on the gas dispersion in a given raw material is investigated using a stainless steel and transparent agitated column with narrow annular gap (NAGU) equipped with right-angle cross paddle impellers or cylinder. Using right-angle cross paddle impeller in NAGU, several configurations are considered by changing: the angle (θ=0°–30°–45°) and the gap (δ=0 or 5 mm) between two successive elements. It is shown that the compact shifted geometry (δ=0 mm; θ=30°) is much more efficient to achieve total gas incorporation than the others. Conversely, the impeller configuration does not seem to influence bubble mean diameter. The mean diameter decreases slightly from 19 μm to 15 μm when the rotation speed increases from 200 rpm to 1600 rpm, whatever the configuration. Qualitative and quantitative aspects of the bubble breakup are investigated using a transparent NAGU. Tip breakup appears to be the predominant dispersion phenomenon in the system.

1. Introduction

Many natural and processed foods consist of dispersions or have been in a dispersed state during their formation. Emulsions and foams are such examples in food industry. Foams are random dispersions of gas phase most often air, but also nitrogen or carbon dioxide into a continuous liquid, semi-liquid or solid phase (Thakur et al., 2003). Food foams contain fat particles, carbohydrates and emulsifiers like proteins, which determine the stability of air bubbles (Rodríguez Patino et al., 2008; Eisner et al., 2007). In spite of numerous applications of foaming process especially in food products such as: bakery, confectionery, meat products, fat-based products, ice cream, dressings, etc. (Goff, 1997; Campbell and Mougeot, 1999), the mechanism of gas dispersion in such products does not take attention of researchers. However gas dispersion in food raw material is not a spontaneous operation. In order to make dispersions, a large amount of mechanical energy must be supplied to increase the interfacial area, however in the absence of surfactant and thickening agent the final dispersion will never produce a foam structure. On the other hand, too rapid stabilization of the interfaces will oppose to the dispersive effects of the mechanical action and block the dispersion. Obviously, the dispersion of gas in such media not only depends on the quantity of energy but also on the way this energy is introduced and distributed into the continuous phase. The structure of the flow generated by paddles is the key parameter for efficient gas dispersion within the continuous phase. For most high viscosity foods involving laminar flows the breakup of bubbles results from the competition between both viscous and capillary effects which are described by the Capillary number *Ca*:

$$Ca = \frac{\eta \dot{\gamma} d}{2\sigma} \quad (1)$$

where η is the viscosity, $\dot{\gamma}$ the shear rate d is the bubble diameter and σ the surface tension. The breakup of bubbles occurs over a critical value of the Capillary number Ca_c (Grace, 1982; Golemanov et al., 2008; Müller-Fischer et al., 2008). Thus, for a fluid with given physico-chemical properties, the minimum bubble diameter is inversely proportional to $\dot{\gamma}$. This parameter seems to be considered as a key parameter to enhance gas dispersion in foaming process. Considering shear rate as a key parameter, two kinds of apparatus are used to produce foams: rotor-stator units (RS) and scraped-surface heat exchangers

* Corresponding author at: Institut Pascal, Clermont Université, ENSCCF, F-63177 Aubiere, Puy de dome, France. Tel.: +33 473405055; fax: +33 473407829.
E-mail address: Djelveh@univ-bpclermont.fr (G. Djelveh).

0009-2509/$ - see front matter © 2012 Published by Elsevier Ltd.
doi:10.1016/j.ces.2012.02.055

Please cite this article as: Souidi, K., et al., Effect of impellers configuration on the gas dispersion in high-viscosity fluid using narrow annular gap unit. Part 1: Experimental approach. Chem. Eng. Sci. (2012), doi:10.1016/j.ces.2012.02.055

(SSHE) (Dickinson and Stainsby, 1982). In both devices, the mixture is run through narrow gaps between a stator and a rotor turning at high speed, resulting in gas dispersion (Djelveh et al., 1994; Djelveh and Gros, 1995; Gonzalez Mendez et al., 1993; Russell et al., 1997). Considering shear rate, the mean shear rate within the first apparatus remains high (Atiemo-Obeng and Calabrese, 2004) while in the second one, the mean shear rate is relatively low. Nevertheless, at the wall, the local shear rate reaches high values because of the scraping blades (Dumont et al., 2000). However, there is actually no rule to define which of them is more convenient to carry out foaming process on a given raw material. Narchi et al. (2007) using a matrix model showed that the effectiveness of foaming varies significantly depending on the method of contact between gas and liquid phases whether one uses a rotor-stator system (RS) or a simplified version of SSHE named Narrow Annular Gap Unit (NAGU), with the same operating conditions. During recent years, our laboratory focused on the continuous foaming process of real formulations (white sauce, ice cream, whipped cream, liver mousse, fresh cheese) (Thakur et al., 2005, 2006; Labbafi et al., 2005; Vial et al., 2006) using NAGU equipped with flat-bladed impellers. These investigations proved that such impellers favor gas dispersion even at low rotational speed, requiring a fairly low level of energy consumption to make food foams, as compared to solid rotors. Authors showed also how to use the Metzner & Otto procedure to determine process viscosity, mean shear rate and how to predict mean bubble diameter for a given raw material. Such investigation was only based on the hypothesis that the mean shear rate was responsible for bubble division. However, inside NAGU, the values of $\dot{\gamma}$ vary in a large range. The highest values of $\dot{\gamma}$ are expected to produce the smaller bubbles but the regions of high shear rate represent a small volume of the column. Two questions may be raised here: (i) which of them ($\dot{\gamma}_{mean}$ or $\dot{\gamma}_{max}$) is pertinent to explain the bubble size population in the foam; (ii) what is the role of impeller design on bubble dispersion within liquid phase.

The aim of our work is to study the flow behavior in such a simple device by imaging and numerical analysis. The composition of the raw material is kept constant and is representative of material used in dairy foaming process. In this first part, the objective is to find out experimentally how the modification of the configuration of paddles affects foaming performance and mechanism of bubble division in such raw material.

2. Materials and methods

2.1. Raw material preparation

Foaming experiments are carried out using a raw material with a viscosity comparable of those used in foaming process. The amount of dehydrated glucose sirup (Glucidex IT 21, Roquette Frères, France) in water is selected to obtain the desired viscosity of the raw material. The foaming agent (2%w/w) consists of a whey protein isolate (Prolacta 90, Lactalis, France) used in food industry because it provides abundant and stable foams. This concentration is used to obtain a model formulation corresponding to foaming raw material. The preparation of the raw material is carried out in a kitchen mixer (Stephan UMC 5, Germany) under vacuum at room temperature. Raw material is then kept overnight for aging which is necessary for total hydration of proteins. After aging, it is characterized in terms of density (ρ), surface tension and rheological properties. The density is obtained by measuring the mass-to-volume ratio in a beaker of known volume. Surface tension is measured K12 tensiometer (Krüss GmbH, Germany) and Wilhelmy's plate method at 20 °C. Viscosity is measured by a stress-controlled rheometer (AR G2, TA instrument, USA) equipped with a 40 mm plate-plate geometry and a Peltier circulator for temperature control. The gap between the plates is set at 0.5 mm and shear rate is varied in the range of 10–1000 s^{-1} at 20 °C. In this range, raw material is Newtonian as it was previously described by Narchi et al. (2009). The composition and the properties of the raw material are given in Table 1.

2.2. Continuous foaming apparatus

The apparatus (Fig. 1(a)), used in the foaming process consists of a jacketed cylindrical stainless steel column, 35 mm in diameter and 140 mm high; designed as NAGU. The device is mechanically stirred using seven right-angle mixing elements of 33 mm diameter (D) and 10 mm high (Fig. 1(b)). The configuration of the impellers can be changed by varying the gap δ and the angle θ between two successive elements (Fig. 1(b)). The different configurations are summarized in Table 2. The NAGU is also used as Couette device using a cylinder of 33 mm diameter as rotor inside the column. The rotation speed of the impeller (N) is varied between 200 rpm and 1600 rpm using a speed-controlled IK LaborTechnik RE-16 engine (Ika-Werke GmbH, Germany). The torque (T) between the shaft and the impeller is measured using an IK MR-D1 system from Ika-Werke GmbH (Germany) during foaming operation. The jacketed column is thermally regulated (20 °C) using a cooling cryo-thermostat WKL-600 (Lauda GmbH, Germany).

The liquid and gas phases are injected co-currently at the bottom of the column using a peristaltic pump and a thermal gas

Table 1
Composition and properties of raw material (%w/w).

Dehydrated glucose	Water	Protein, WPI	Density (kg/m^3)	Viscosity (Pa s)	Surface tension (N/m)
62	36	2	1280	1.65	0.050

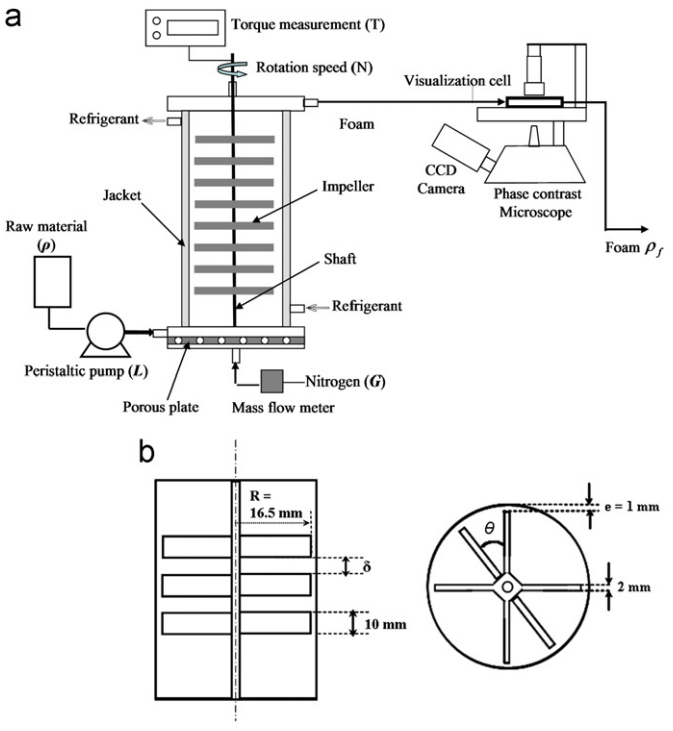

Fig. 1. (a) Schematic diagram of experimental setup. (b) Flat-bladed impellers of the narrow annular gap agitated column (NAGU).

Please cite this article as: Souidi, K., et al., Effect of impellers configuration on the gas dispersion in high-viscosity fluid using narrow annular gap unit. Part 1: Experimental approach. Chem. Eng. Sci. (2012), doi:10.1016/j.ces.2012.02.055

Table 2
Configurations of impeller used in continuous foaming operation.

Configuration	Compact (δ=0 mm)	Spread (δ=5 mm)
Aligned (θ=0°)	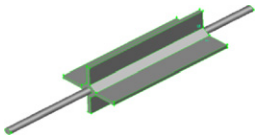	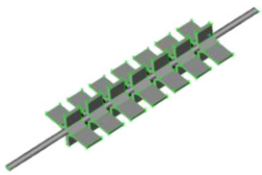
Shifted (θ=30° or 45°)	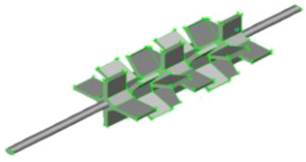	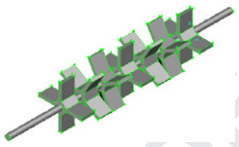

mass flow meter (Brooks Instr. Co., USA), respectively. The gas volume fraction in the inlet stream ε_{inlet} is then calculated from the liquid and gas volumetric flow rate:

$$\varepsilon_{inlet} = \frac{G}{G+L} \quad (2)$$

At the top of the column, foam is divided in two streams. The first one is used to measure the foam density ρ_f with an accuracy of $\pm$2%. The gas volume fraction of the foam is thus given by the following relation:

$$\varepsilon = \frac{\rho-\rho_f}{\rho} \quad (3)$$

Overrun can also be used to evaluate the amount of gas incorporated in the foam:

$$Overrun = \frac{\rho-\rho_f}{\rho_f} \times 100 \quad (4)$$

gas fraction of the foam and *Overrun* are related according to the following equation:

$$Overrun = \varepsilon\frac{\rho}{\rho_f} \times 100 \quad (5)$$

In this work, gas fraction will be used as it presents more realistic information on the gas incorporation.

The second stream passes through an online image analysis system consisting of a CCD camera (Kappa Opto-electronics GmbH, Germany) coupled to a microscope (Axiovert-25, Carl Zeiss Jena GmbH, Germany). For each set of operating conditions the diameter of at least 400 bubbles is measured with an accuracy of $\pm$5%. The mean diameter of bubbles is calculated by dividing the sum of bubbles diameters by the number of bubbles.

A transparent column (Fig. 2) has also been designed to study the flow pattern of bubbles through different impeller configurations and bubble breakup under constant shear rate. The column is filled with raw material. A rectangular transparent box filled with the same raw material is mounted around the column to avoid light diffraction due to the circular shape of the cylinder. Air bubbles are injected by means of a syringe connected to a capillary tube of internal diameter equal to 180 μm (Postnova Analytics Inc, USA). The gas volumetric flow rate is controlled by a syringe-pump (KD scientific, USA). Images of the bubbles are recorded by mean of a JAI-Pulnix GigE camera (Edmund Optics Inc. USA) at 150 fps. Two types of experiments have been set-up.

The column is first equipped with transparent cross paddles similar to the ones used in the stainless steel column, in order to show how the configuration of impellers modifies the trajectory of bubbles within the cylinder.

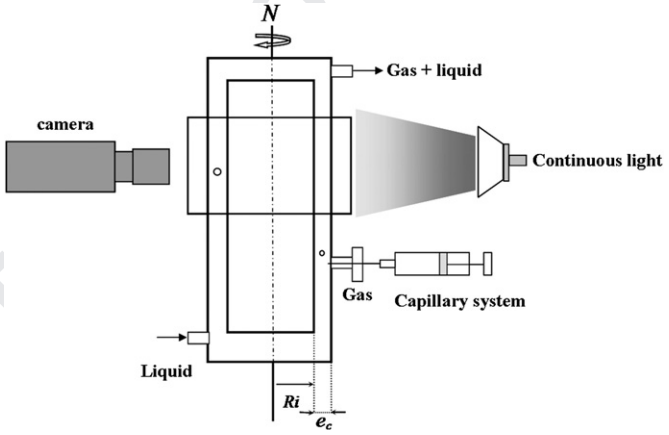

Fig. 2. Experimental setup designed to generate bubble with constant diameter and to study bubble breakup under constant shear rate (Couette system) or the flow pattern of bubbles using transparent impeller with configuration similar to the one presented in Table 2.

Then, the column is equipped with a transparent cylinder of 33 mm diameter (as a rotor) to obtain a Couette device (Fig. 2), so that bubble breakup under constant shear rate can be observed. In order to keep a constant optical index, the internal cylinder is also filled with the same raw material. To determine the initial bubble diameter *d*, an image is taken in the absence of rotation speed. It must be mentioned that all the bubbles generated with the syringe are smaller than the gap ($e_{couette}$) between two cylinders and their diameter remains between $0.25e_{couette}$ and $0.4e_{couette}$. During the experiment, care has been taken to check that the bubbles are not in contact with the wall of cylinders. Then, the images of bubbles are recorded at different rotation speeds; the aim is to determine the minimum value of shear rate corresponding to bubble breaking. As the gap between the two cylinders $e_{couette}$ is weak compared to the radius of the internal cylinder ($e_{couette}/R_i$=0.12), the rotation of the internal cylinder creates a couette flow of constant shear rate $\dot{\gamma}$ given by:

$$\dot{\gamma} = \frac{2\pi R_i N}{e_{couette}} \quad (6)$$

3. Results and discussion

To study the impact of the impeller configurations (Table 2) on the foaming performance, two parameters have been quantified: efficiency of foaming and bubble diameter (mean and size distribution). Experiments on the transparent column bring

Please cite this article as: Souidi, K., et al., Effect of impellers configuration on the gas dispersion in high-viscosity fluid using narrow annular gap unit. Part 1: Experimental approach. Chem. Eng. Sci. (2012), doi:10.1016/j.ces.2012.02.055

information on the flow pattern of bubbles in each configuration and on the dominant bubble break-up mechanism. Couette device allows quantifying the threshold of breakup in a simple shear flow. However, as the hypothesis of laminar flow governs the above investigation; we first assure the validity of this hypothesis.

3.1. Flow regime

The relation between *Ne* (Newton number) and *Re* (Reynolds number) is always given by:

$$Ne = \beta Re^{-\alpha} \tag{7}$$

where the two dimensionless numbers *Re* and *Ne* are defined as:

$$Re = \frac{ND^2\rho}{\eta} \tag{8}$$

and

$$Ne = \frac{P}{D^5N^3\rho} \tag{9}$$

The parameter β depends on the configuration of the impeller while α determines flow regime. Especially in laminar flow, α is always close to 1. The experimental procedure for the determination of α and β in our cases consists of measuring for each configuration, torque on the shaft of the impeller under different rotation speed N without (T_0) and with the raw material (T_L) inside the column. Power consumption (P) is obtained using the following relation.

$$P = 2\pi N(T_L - T_0) \tag{10}$$

For a solution with given physical properties (ρ,η), it is then possible to determine *Re* and *Ne* numbers for each rotation speed. The evolution of *Ne* versus *Re* number is given on Fig. 3 for the four impeller configurations used in this work. ~~For the all configurations,~~ Table 3 shows that the parameter α is close to 1 ($ReNe \approx \beta$) indicating that the flow regime remains laminar for the operating conditions used here. As a result, Eq. (7) shows that under constant *Re* number, the *Ne* number, which also represents power consumption in the apparatus, only depends on the coefficient β. Moreover, Table 3 shows that β values change by changing the configuration of impellers. It seems that the level of power consumption (β) differs significantly between these configurations. It is then interesting to note that the highest value of β, indicating highest power consumption, is not correlated to the foaming performance. The highest value of β=2264 is indeed obtained when the impellers are configured with: δ=5 mm; θ=0° while the best performance in foaming efficiency is obtained

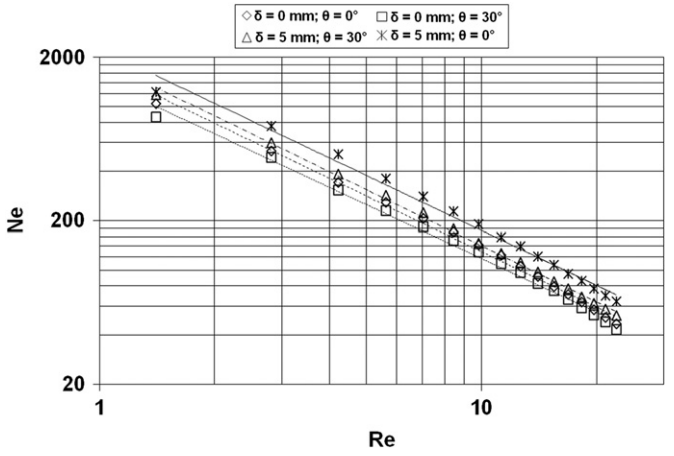

Fig. 3. Newton number versus Reynolds number for the different impeller configurations.

Table 3
Fitted parameters obtained from *Ne* versus *Re* experimental points.

Configuration	Compact (δ=0 mm)		Spread (δ=5 mm)	
Aligned (θ=0°)	α	1.1	*A*	1.1
	β	1724	*B*	2264
	R^2	0.994	R^2	0.990
Shifted (θ=30°–45°)	α	1.1	α	1.1
	β	1451	β	1928
	R^2	0.994	R^2	0.998

when the impellers are configured with: δ=0 mm; θ=30°, see Section 3.2.1. Interestingly in this last configuration, β takes the lowest value indicating the decrease in power consumption compared to the other configurations. Thus, the question to be answered is not how much energy is introduced to the device but rather how energy is locally distributed along the dispersion device. This seems to depend on the design and configuration of impellers within the apparatus.

3.2. Foaming performances in the stainless steel NAGU

Experiments have been conducted using raw material with L=30 mL/min and G=~~10~~ 30 mL/min, 50 mL/min, and 70 mL/min under a range of rotation speed between 200 rpm and 1600 rpm.

3.2.1. Effect of the impellers configuration on foaming efficiency

The influence of the impeller configurations (Table 2) on the foaming efficiency *Eff*

$$Eff = \frac{\varepsilon}{\varepsilon_{\text{inlet}}} \tag{11}$$

is considered for the different rotation speeds and gas to liquid flow ratios.

The variation of the foaming efficiency *Eff* versus the rotation speed N is plotted on Fig. 4 for different shifted angles θ. Due to symmetry considerations, the angle between two successive impellers is varied from 0° to 45°. For the compact geometry (Fig. 4(a)), experimental results show that at low values of N (200 rpm and 400 rpm), the efficiency is close to 1 whatever the angle θ. For a rotation speed greater than 400 rpm, the aligned geometry (θ=0°) only allows a partial incorporation of gas. In addition, the efficiency decreases drastically at high rotation speed and falls to approximately 30%. At this stage, blow-by phenomena are gradually induced and are responsible for the decrease of *Eff*. However, when the paddles are shifted, the incorporation of gas is enhanced whatever the rotation speed. The efficiency increases with increasing θ and reaches a maximum value for θ=30°. For both compact and spread configurations, Fig. 4 shows that the incorporation of gas in the liquid phase is also enhanced by shifting the paddles.

Fig. 4(a) and (b) also present the influence of the gap on the foaming efficiency. It appears that *Eff* is always higher in the compact configuration independently of the shifted angle. Accordingly, the gap between two impellers has to be avoided in foaming process. This result can be explained by an accumulation of the bubbles in the gap between impellers which probably promotes the coalescence of the bubbles and thus the formation of gas pockets. It is interesting to note that for all configurations except the compact geometry with θ=30°, the efficiency decreases when the rotation speed increases. One can consider that the depression around the shaft increases while increasing N, and thus promotes the bubble migration and accumulation toward the center of the column. Furthermore, the shear rate is generally lower in this region which limits the breakup of bubbles. Consequently, the bubbles accumulated in this area are

Please cite this article as: Souidi, K., et al., Effect of impellers configuration on the gas dispersion in high-viscosity fluid using narrow annular gap unit. Part 1: Experimental approach. Chem. Eng. Sci. (2012), doi:10.1016/j.ces.2012.02.055

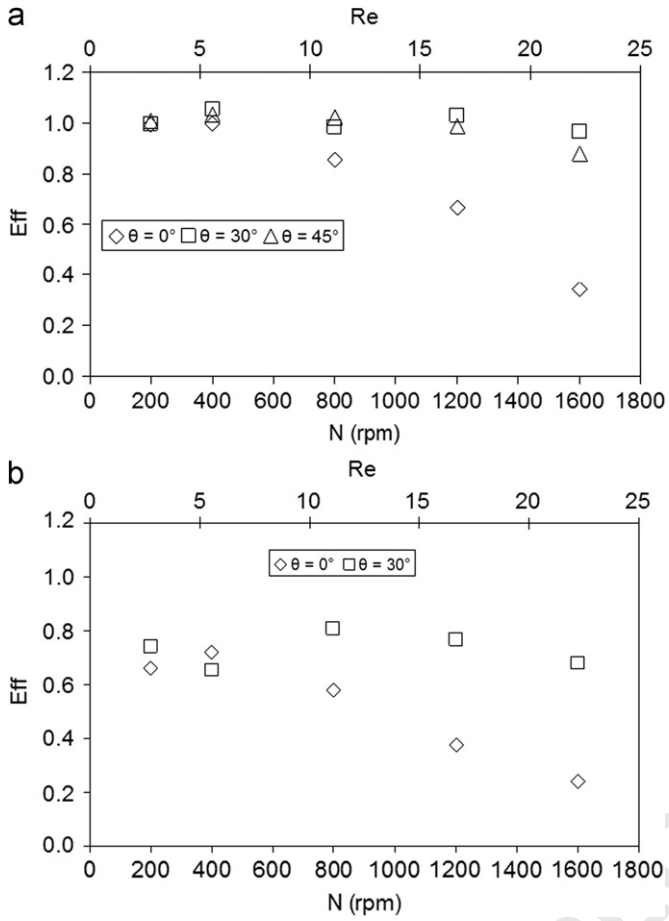

Fig. 4. Foaming efficiency versus rotation speed for $L=30$ mL/min and $G=10$ mL/min; (a) compact geometry ($\delta=0$ mm) (b) spread geometry ($\delta=5$ mm).

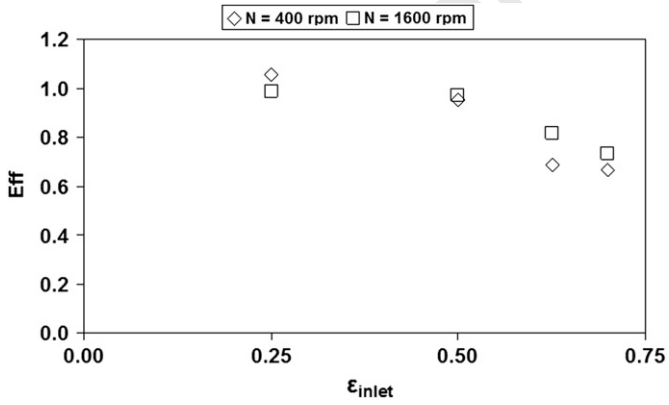

Fig. 5. Foaming efficiency as function of inlet gas fraction for the compact geometry ($\delta=0$ mm) with shifted paddle ($\theta=30°$).

slightly (or not) submitted to division and contribute to the formation of gas pockets.

As a conclusion, the compact geometry with an angle of 30° corresponds to an optimal configuration for total incorporation of the gas injected inside the column ($Eff=1$).

Fig. 5 presents the variation of Eff as function of inlet gas volume fraction (ε_{inlet}) for the rotation speed $N=400$ rpm and 1600 rpm. Using the optimal impeller configuration ($\delta=0$ mm; $\theta=30°$) for $G/L=30/30$ (mL/min) corresponding to the $\varepsilon_{inlet}=50\%$, total incorporation of gas is achieved ($Eff=1$) for both rotation speeds. When the inlet gas volume fraction increases from $\varepsilon_{inlet}=62.5\%$ to 70% (corresponding to gas volumetric flow rate of 50 mL/min to 70 mL/min), the efficiency decreases whatever the rotation speed. It should be noted that the residence time has an effect on gas dispersion but the aim of this figure is to quantify to which extent the above configuration could incorporate gas volume fraction even by decreasing the residence time. This experimental result also suggests that a fraction of inlet gas goes through a region where the shear rate remains low and consequently induces the formation of gas pockets at the exit of the column. Our results are in agreement with the suggestions of Narchi et al. (2011). Authors mentioned that when high N is combined to high gas flow rate, the effect of centrifugal forces is superimposed over the influence of the local distribution of shear, which finally gives far lower efficiency for gas dispersion.

3.2.2. *Influence of the impellers configuration on mean bubble diameter*

It must be mentioned that for both impeller configurations and Couette cylinder, the bubble size distribution remains monomodal and the probability density function of the bubble diameter is well described by a normal distribution (Fig. 6).

The mean bubble diameter d_{mean} and the standard deviation SD as a function of rotation speed are plotted on Fig. 7 for both compact (a) and spread (b) configurations. This figure shows that the bubble size population is independent of the impeller configuration. The mean diameter monotonically decreases slightly from 18 μm to 15 μm when increasing the rotation speed and thus the viscous stress, while SD is stable around 3 μm. One way of quantifying the performance of impellers for gas dispersion is to study the proportionality between the Sauter mean diameter d_{32} and the maximum bubble diameter d_{max}. The slope equal to 1, implies that the mean diameter is equal to the maximum bubble diameter, and therefore that the bubble fragmentation is uniformly distributed within the foam. Zhou and Kresta (1998) found that the slope value for agitated tanks and bent tubes equipped with a static mixer is between 0.38 and 0.7. Fig. 8 shows that $d_{32}=0.63d_{max}$ which demonstrates that the homogeneity of the bubble size distribution in NAGU is close to that obtained in an efficient agitated tank equipped with a static mixer. However, this value is smaller than that observed in chaotic systems (Habchi et al., 2009).

3.3. *Qualitative and quantitative aspects of bubble division*

The images presented in this section are obtained on the set-up described on Fig. 2 using transparent device with either right-

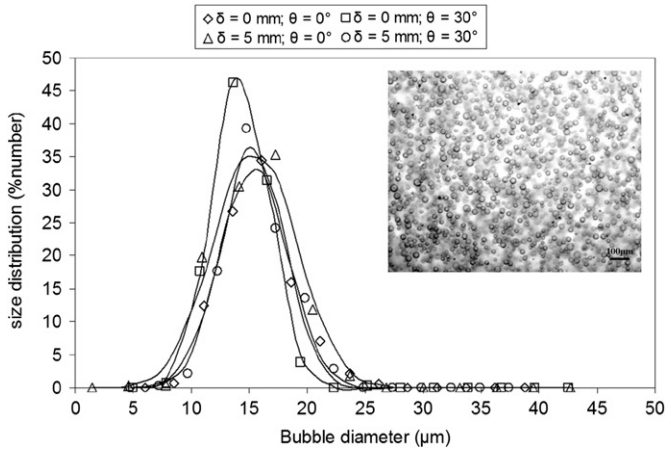

Fig. 6. Bubble size distribution for different impeller configuration (symbols) fitted by a normal distribution (straight lines) for $N=1600$ rpm, $L=30$ mL/min and $G=10$ mL/min. Upper figure: bubble image at the same operating conditions.

Please cite this article as: Souidi, K., et al., Effect of impellers configuration on the gas dispersion in high-viscosity fluid using narrow annular gap unit. Part 1: Experimental approach. Chem. Eng. Sci. (2012), doi:10.1016/j.ces.2012.02.055

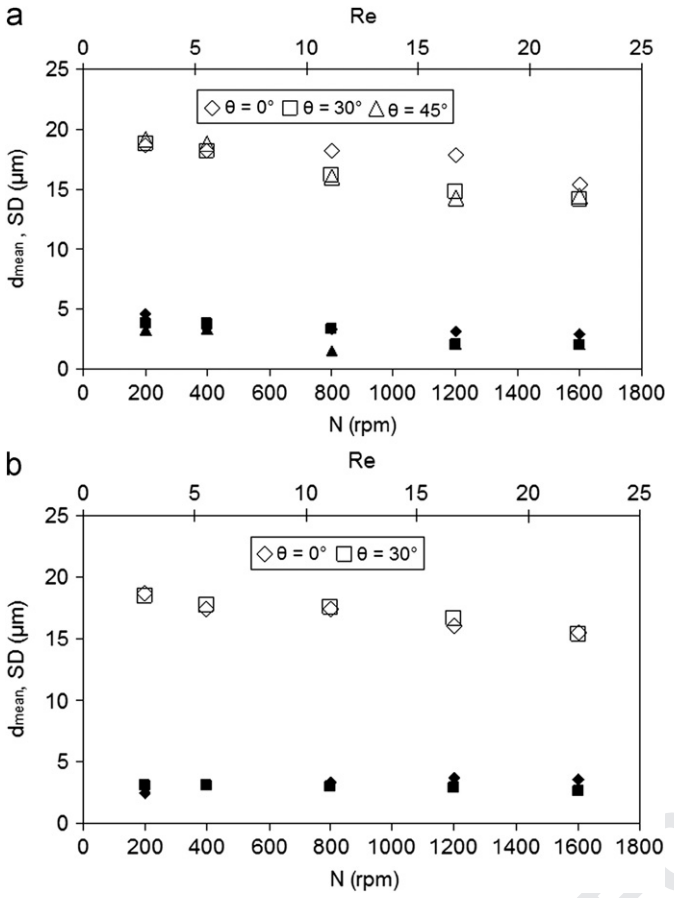

Fig. 7. Mean diameter (open symbols) and standard deviation (dark symbols) of the bubble size distribution function of the speed rotation for L=30 mL/min and G=10 mL/min. (a) Compact configuration (δ=0 mm). (b) Spread configuration (δ=5 mm).

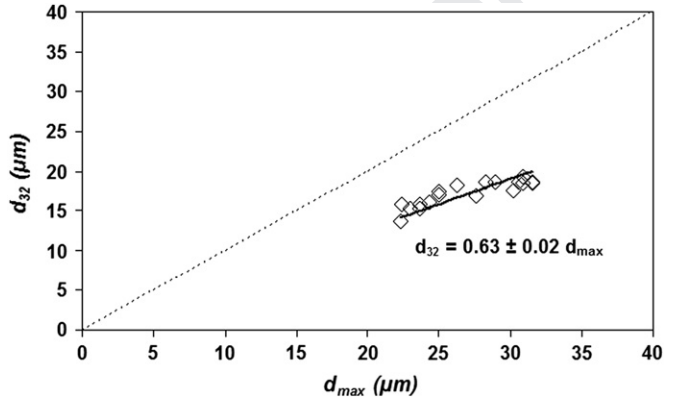

Fig. 8. Sauter mean diameter versus maximum bubble diameter in the NAGU.

angle cross paddle impellers or transparent cylinder as rotor. A first analysis with real impeller system gives qualitative information on the flow pattern generated by the different impeller geometries in order to better understand the difference observed at the process scale. A second analysis with Couette system provides more quantitative information on the bubble rupture.

3.3.1. *Effect of the impellers configuration on bubble dispersion*

Dispersion phenomena at same rotation speed for each impeller configuration can be qualitatively analyzed with the help of Fig. 9. The first observation to be made on this figure is that independently of the configuration, it seems that tip breakup seems the main mechanism for bubble division. That is why this breakup phenomenon will be further detailed in Section 3.3.2.

When using the compact-aligned configuration (δ=0 mm; θ=0°), the bubble dispersion occurs essentially in a small volume between impeller head and the wall. However, in the large volume between the paddles, bubbles are just merely deformed. When a clearance is added between two consecutive impellers (aligned or shifted), the bubbles are relaxed because shear rate is reduced in this gap. Consequently, the dispersion of bubbles is very poor in this area. This could explain the lowest efficiency of spread geometry.

When using the shifted compact configuration (δ=0 mm; θ=30°), a new deformation inducing breakup of bubbles appears due to the angle between the two successive impellers. Following the trajectory of an isolate bubble under given rotation speed, the Fig. 10 shows that the shifted impellers impose a well-defined trajectory from deformation to breakup (Fig. 10(a)–(d)). It seems that such configuration not only reduces the dead-volumes within the column but also favors the bubble division. Such behavior could explain the highest foaming efficiency of the shifted configurations.

The observation of the dispersion phenomena with the different configuration highlights how the distribution of bubbles in the column has an impact on the foaming efficiency. If a gas fraction is imprisoned in a region of low shear rate (center of the column for compact configuration; clearance between two mixing elements for spread configuration), it is not subject to division. This contributes to form gas pockets inducing blow-by phenomena and reduction of efficiency. The compact/shifted configuration is then the only one to distribute properly the bubbles in the media so that all of them can divided (Fig. 4).

3.3.2. *Mechanism of bubble division*

In laminar flows, the bubble deformation depends on the Capillary number Ca, the ratio λ corresponding to the gas to liquid viscosity and also on the concentration of surfactant (De Bruijn, 1993; Stone, 1994). For a given surfactant concentration and a given λ, the bubble deformation increases when increasing Ca. Over a critical value corresponding to Ca_c, the bubble breaks into smaller bubbles. Two types of breakup have been observed (Grace, 1982; Fradette et al., 2006): a total breakup (or burst) and a tip breakup. The tip breakup (or tip streaming) occurs in the presence of surfactant and for a low value of Ca whereas the total breakup is observed for much higher values (Fig. 11).

In the present study, our attention is first focused on determining Ca_c in a simple shear flow by changing λ from 10^{-6} to 10^{-5}. Experiments consist of observing the behavior of a single unconfined ($d < e_{couette}$) bubble in the transparent Couette system under different shear rates. Image analysis reveals that in the range of shear rate investigated, the breakup mechanism is the tip streaming (Fig. 12(a)). For confined bubbles ($d \gg e_{couette}$) tip breakup is also observed (Fig. 12(b)). The size of confined bubbles is reduced by successive breakup, producing bubble dispersion into the continuous phase. Here, the gas fraction of the foam produced by the bubble dispersion does not exceed 10% and the bubble diameters are much smaller than the gap. The values of Ca_c as function of λ are plotted on Fig. 11. It appears that Ca_c keeps constant around 0.3. This value is close to that measured by Grace (1982) for drop tip breakup. According to the experimental values of Ca_c for $10^{-7} < \lambda < 10^{-6}$ (Müller-Fischer et al., 2008), the values obtained here suggest that Ca_c decreases from 40 to 0.3 for λ increasing from ~~6.72.10^{-6}~~ to 6.10×10^{-5}. In addition, it is interesting to note that the values of Ca_c for the bubble breakup in foam (Golemanov et al., 2008) are close to those obtained using continuous flow. For a given shear rate, the minimum bubble

Please cite this article as: Souidi, K., et al., Effect of impellers configuration on the gas dispersion in high-viscosity fluid using narrow annular gap unit. Part 1: Experimental approach. Chem. Eng. Sci. (2012), doi:10.1016/j.ces.2012.02.055

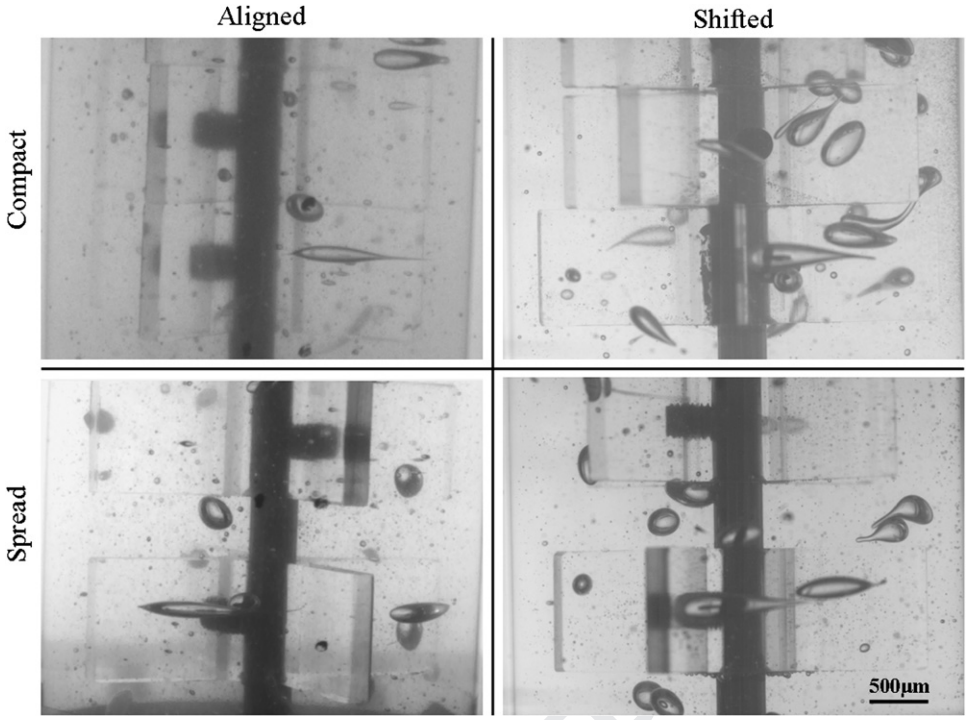

Fig. 9. Visualization of the bubble dispersion in the different impeller configurations.

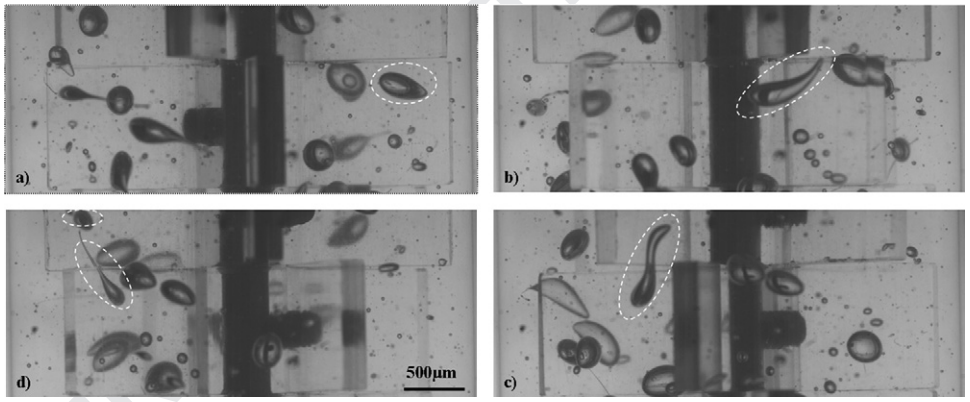

Fig. 10. Detailed trajectory of an isolated bubble (white dashed line) under given rotational speed (200 rpm): (a) nearly spherical bubble close to the paddle, (b) deformation when the bubble approaches the upper impeller, (c) increased deformation in the shifted area, (d) bubble breakup to daughter bubbles.

diameter under which there is no more tip breakup is given by:

$$d_c = \frac{2Ca_c\sigma}{\eta\dot{\gamma}} \tag{12}$$

Using the experimental value of Ca_c (0.3), the calculated critical bubble diameter d_c is plotted as a function of $\dot{\gamma}$ on Fig. 13. In the range of the shear rate investigated, d_c decreases monotonically from 220 μm to 6 μm.

3.3.3. Comparison of critical bubble diameter with mean bubble diameter

The critical bubble diameter is helpful to understand the results on mean bubble diameter obtained over the range of shear rate investigated. The mean diameter of bubbles obtained in Section 3.2 and NAGU as Couette system (metal cylinder instead of flat-bladed impellers) are also reported in Fig. 13. It should be noted that the values of d_{mean} for device equipped with flat-bladed impellers are plotted for $\dot{\gamma} = \dot{\gamma}_{max}$, where $\dot{\gamma}_{max}$ is the shear rate at the tip of the paddles:

$$\dot{\gamma}_{max} = \frac{2\pi RN}{e} \tag{13}$$

The comparison between d_{mean} and d_c in both devices (Couette cylinder and flat-bladed impellers) shows that for $\dot{\gamma} < 400\ s^{-1}$, $d_{mean} \ll d_c$. This result confirms that the tip streaming is the dominant breakup mechanism. The size of injected bubbles (higher than d_c) is indeed gradually reduced by successive tip breakups up to the critical diameter. As the daughter bubbles are much smaller and more numerous, the overall mean bubble diameter is lower than d_c. When $\dot{\gamma}$ is over $400\ s^{-1}$, the mean diameter for both Couette cylinder and flat-bladed impellers reaches a constant value and thus the difference between d_{mean} and d_c reduces when increasing $\dot{\gamma}$. Such behavior suggests that over a critical value of shear stress, the mother bubbles diameter get closer to the daughter diameter. This explains that mean bubble diameter is not very sensitive to rotation speed in the range of investigated (Fig. 7). For the flat-bladed impellers, we observe that d_{mean} becomes higher than d_c for $\dot{\gamma} > 2000\ s^{-1}$. Two

Please cite this article as: Souidi, K., et al., Effect of impellers configuration on the gas dispersion in high-viscosity fluid using narrow annular gap unit. Part 1: Experimental approach. Chem. Eng. Sci. (2012), doi:10.1016/j.ces.2012.02.055

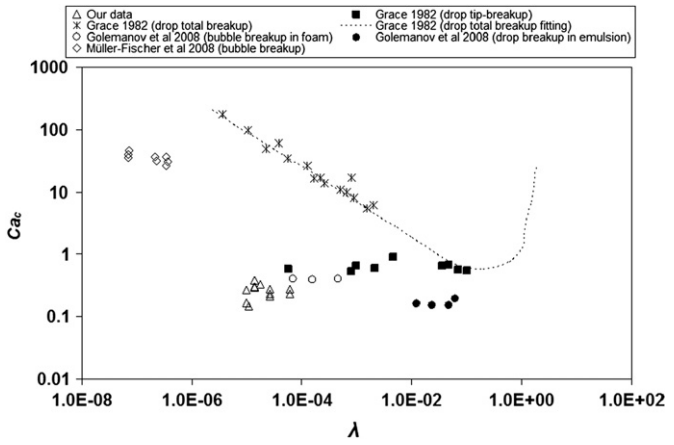

Fig. 11. Critical Capillary number for bubbles (open symbols) and drops (dark symbols) in a simple shear flow, as function of viscosity ratio. (△) tip-breakup (our data); (◇) tip breakup (Müller-Fischer et al., 2008); breakup in simple shear flow (○) bubbles in foam ($\varepsilon \geq 92\%$) and (●) drops in emulsion ($\Phi \geq 80\%$) from Golemanov et al. (2008); (■) drop tip-breakup and (✳) drop total breakup by Grace (1982).

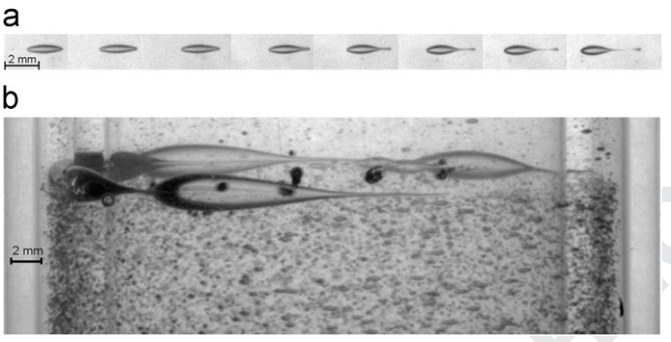

Fig. 12. Images of bubbles in the Couette system. (a) tip streaming function of time for an isolated bubble. (b) Tip streaming for bubbles in the gas dispersion and (c) foaming formation from one large initial bubble.

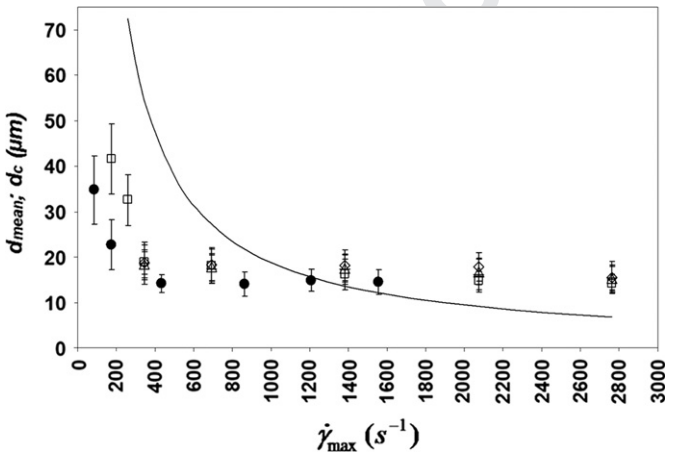

Fig. 13. Bubble mean diameter versus rotation speed. (◇) $\delta=0$ mm; $\theta=0°$; (□) $\delta=0$ mm; $\theta=30°$; (△) $\delta=5$ mm; $\theta=30°$; (+) $\delta=5$ mm; $\theta=0°$ and (●) cylinder. The continuous line represents the critical bubble diameter calculated from Eq. (11). Vertical bars correspond to standard deviation.

hypotheses can be formulated to explain such behavior: (i) high rotation speed needed to obtain high shear rate induces strong mixing of the foam which promotes the random collision between bubbles. As a consequence, the bubble size distribution results from the competition between breakup and coalescence. (ii) When increasing N, the depression at the center of the column increases inducing bubbles accumulation in this region. On the other hand, high rotation speed induces centrifugal forces that favor gas and liquid separation due to their density differences. A gas cone could then be generated around the rotor preventing the gas phase to be dispersed in the liquid phase. Consequently, there are less and less bubbles in the gap between impeller head and column wall, region of highest shear rates.

The comparison between the mean diameter in the Couette device and the NAGU equipped with flat-bladed impellers shows that the Couette device always produces the smallest bubbles. This result is not surprising as the highest region of shear rate in the NAGU equipped with flat-bladed impellers represents only a small volume of the column. Nevertheless, their difference reduces when increasing $\dot{\gamma}$, and for $\dot{\gamma} > 300\ s^{-1}$, their values become very close. This result means that $\dot{\gamma}_{max}$ is responsible for the bubble size distribution observed when $\dot{\gamma} > 300\ s^{-1}$.

4. Conclusion

The present work shows that the impeller configuration plays a key role on the gas entrapment in the continuous phase. The significant effect of impeller configuration on the foaming efficiency can be linked to a modification of flow pattern. Shifted paddles enhance the mixing efficiency whereas the gap between paddles creates zones of reduced shear stress which promote the coalescence.

Contrary to the foaming efficiency, the bubble size distribution is independent of the impeller configuration and the bubble mean diameter decreases slightly compared to the range of rotation speed investigated. Detailed investigation of the bubble breakup in both NAGU and Couette systems reveals that tip streaming is the dominant breakup mechanism which explains the possibility to disperse gas even at low rotation speed and the relative independence of mean bubble diameter to the rotation speed. It also emphasizes the effect of the configuration of impeller on the distribution of bubbles within the column. The values of the critical capillary number have been determined for a viscous ratio λ ranging from 10^{-6} to 10^{-5}. The values observed are close to those obtained by Grace (1982) in drop breakup and to those obtained by Golemanov et al. (2008) for bubbles breakup in foams.

Using experimental Ca_c, the critical diameter has been determined in the range of shear rate investigated. At low shear rate, the comparison between the mean diameter and the critical diameter shows that $d_{mean} \ll d_c$ which confirms the occurrence of tip breakup. On the contrary, at high shear rate, d_{mean} becomes greater than d_c. This interesting result could be explained by the bubble coalescence or the impoverishment of gas phase in the region of highest shear stress. The bubble size in a Couette system is always lower than in the NAGU equipped with flat-bladed impellers when taking $\dot{\gamma} = \dot{\gamma}_{max}$, which can reasonably be explained by the small volume of highest shear rate regions compared to the total volume of the NAGU column. Nevertheless, the mean diameters quickly collapse when increasing $\dot{\gamma}$, indicating that $\dot{\gamma}_{max}$ is responsible for the bubble size distribution observed.

As a conclusion, the NAGU used in this work seems to be a convenient device to perform foaming under steady-state flow conditions. The device is very simple to design compared to rotor/stator units. However the performance of such device also depends on the configuration of impellers within the stator. The example treated in this paper emphasizes the importance of such investigation in foaming process. Indeed, in spite of the same shear rate given by Couette system and NAGU equipped with flat-bladed impellers, it is never possible to obtain a foam structure in

Please cite this article as: Souidi, K., et al., Effect of impellers configuration on the gas dispersion in high-viscosity fluid using narrow annular gap unit. Part 1: Experimental approach. Chem. Eng. Sci. (2012), doi:10.1016/j.ces.2012.02.055

a Couette system even by increasing the shear rate. This highlights the importance of the impeller configuration on flow pattern that remains the key parameter for successful foaming process.

Nomenclature

d	bubble diameter (m)
d_{max}	maximum bubble diameter (m)
d_{mean}	mean bubble diameter (m)
d_{32}	Sauter bubble diameter (m)
d_c	critical bubble diameter (m)
D	impeller diameter (m)
Eff	foaming efficiency
$e_{couette}$	gap between the two cylinders (m)
G	gas volume flow rate (m^3/s)
L	liquid volume flow rate (m^3/s)
N	rotation speed (rps)
R_i	radius of internal cylinder (m)
P	power dissipated (W)
SD	standard deviation
T_0	torque measured without raw material (N m)
T_L	torque measured in the presence of raw material (N m)

Dimensionless numbers

Ca	capillary number Eq. (1)
Ca_c	critical Capillary number
Ne	Newton number Eq. (9)
Re	Reynolds number Eq. (8)
λ	gas to liquid viscosity ratio

Greek letters

α	regime flow index
β	energy level index
δ	gap between two successive impellers (m)
θ	shift angle between two successive impellers (degree)
η	dynamic viscosity (Pa s)
ρ	density of raw material ($kg\,m^{-3}$)
ρ_f	foam density ($kg\,m^{-3}$)
σ	surface tension ($N\,m^{-1}$)
$\dot{\gamma}$	shear rate (s^{-1})
$\dot{\gamma}_{mean}$	mean shear rate (s^{-1})
$\dot{\gamma}_{max}$	maximum shear rate (s^{-1})
ε	gas volume fraction
ε_{inlet}	Inlet gas volume fraction
Φ	dispersed phase volume fraction in emulsions

References

Atiemo-Obeng, V., Calabrese, R.V., 2004. Rotor-stator mixing devices. In: Paul, E.L., Atiemo-Obeng, V., Kresta, S.M. (Eds.), Handbook of Industrial Mixing: Science and Practice. John Wiley and Sons, Hoboken, NJ, USA.

Campbell, G.M., Mougeot, E., 1999. Creation and characterization of aerated food products. Trends Food Sci. Technol. 10, 283–296.

De Bruijn, R.A., 1993. Tip streaming of drops in simple shear flows. Chem. Eng. Sci. 48, 277–284.

Dickinson, I.E., Stainsby, G., 1982. Colloids in Food. Applied Science Publishers, London, New York.

Djelveh, G., Bacati, O., Gros, J.B., 1994. Mechanical aspects of gas dispersion in continuous foaming food processes using scraped surface heat exchangers. J. Food Eng. 23, 213–223.

Djelveh, G., Gros, J.B., 1995. Estimation of physical properties of foamed foods using energy dissipation in scraped surface heat exchangers. J. Food Eng. 26, 45–55.

Dumont, E., Fayolle, F., Legrand, J., 2000. Flow regimes and wall shear rates determination within a scraped surface heat exchanger. J. Food Eng. 45, 195–207.

Eisner, M.D., Jeelani, S.A.K., Bernhard, L., Windhab, E.J., 2007. Stability of foams containing proteins, fat particles and non-ionic surfactants. Chem. Eng. Sci. 62, 1974–1987.

Fradette, L., Li, H.-Z., Choplin, L., Tanguy, P.A., 2006. Gas/liquid dispersions with a SMX static mixer in the laminar regime. Chem. Eng. Sci. 61, 3506–3518.

Goff, H.D., 1997. Colloids aspects of ice cream – a review. Int. Dairy J. 7, 363–373.

Golemanov, K., Tcholakova, S., Denkov, N.D., Ananthapadmanabhan, K.P., Lips, A., 2008. Breakup of bubbles and drops in steadily sheared foams and concentrated emulsions. Phys. Rev. E 78, 051405-1–051405-11.

Gonzalez Mendez, N.F., Djelveh, G., Gros, J.B., 1993. Performance of scraped surface heat exchangers in foaming food process. Lebensmittelwissenshaft 26, 538–543.

Grace, H.P., 1982. Dispersion phenomena in high viscosity immiscible fluid systems and application of static mixers as dispersion devices in such systems. Chem. Eng. Comm. 14, 225–277.

Habchi, C., Lemenand, Th., Della Valle, D., Peerhossaini, H., 2009. Liquid/liquid dispersion in a chaotic advection flow. Int. J. Multiphase Flow 35, 485–497.

Labbafi, M., Bouaouina, H., Vial, Ch., Djelveh, G., Picgirard, L., Casalinho, J., Schorsch, C., 2005. Impact of technology and whipping conditions on dairy topping fabrication. Sci. Aliments 25, 381–398.

Müller-Fischer, N., Tobler, Ph., Dressler, M., Fischer, P., Windhab, E.J., 2008. Single bubble deformation and breakup in simple shear flow. Exp. Fluids 45, 917–926.

Narchi, I., Vial, Ch., Labbafi, M., Djelveh, G., 2007. Influence of bulk and interfacial properties and operating conditions on continuous foaming operation applied to model media. Food Res. Int. 40, 1069–1079.

Narchi, I., Vial, Ch., Djelveh, G., 2009. Effect of protein–polysaccharide mixtures on the continuous manufacturing of foamed food products. Food Hydrocolloids 23, 188–201.

Narchi, I., Vial, Ch., Djelveh, G., 2011. Comparative study of the design of continuous aeration equipment for the production of food foams. J. Food Eng. 102, 105–114.

Rodríguez Patino, J.M., Carrera Sánchez, C., Rosario Rodríguez Niño, Ma., 2008. Implications of interfacial characteristics of food foaming agents in foam formulations. Adv. Colloid Interface Sci. 140, 95–113.

Russell, A.B., Burmester, S.S.H., Winch, P.J., 1997. Characterization of shear thinning flow within a scraped surface heat exchanger. Trans. Inst. Chem. Eng. 75, 191–197.

Stone, H.A., 1994. Dynamics of drop deformation and breakup in viscous fluids. Annu. Rev. Fluid Mech. 26, 65–102.

Thakur, R.K., Vial, Ch., Djelveh, G., 2003. Influence of operating conditions and impeller design on the continuous manufacturing of foam foods. J. Food Eng. 60, 9–20.

Thakur, R.K., Vial, Ch., Djelveh, G., 2005. Combined effects of process parameters and composition on foaming of dairy emulsions at low temperature in an agitated column. J. Food Eng. 60, 9–20.

Thakur, R.K., Vial, Ch., Djelveh, G., 2006. Effect of pH of food emulsions on their continuous foaming using a mechanically agitated column. Innovative Food Sci. Emerg. Technol. 7, 203–210.

Vial, Ch., Thakur, R.K., Picgirard, L., Djelveh, G., 2006. Continuous manufacturing of a light-textured foamed fresh cheese by dispersion of a gas phase. I. Influence of process parameters. J. Food Eng. 77, 1–13.

Zhou, G., Kresta, S.M., 1998. Correlation of mean drop size and minimum drop size with the turbulence energy dissipation and the flow in an agitated tank. Chem. Eng. Sci. 53, 2063–2079.

Please cite this article as: Souidi, K., et al., Effect of impellers configuration on the gas dispersion in high-viscosity fluid using narrow annular gap unit. Part 1: Experimental approach. Chem. Eng. Sci. (2012), doi:10.1016/j.ces.2012.02.055